High-frequency nanofluidics: a universal formulation of the fluid dynamics of MEMS and NEMS

K. L. Ekinci,*[ab] V. Yakhot,[a] S. Rajauria,[b] C. Colosqui[ac] and D. M. Karabacak[ad]

Received 1st March 2010, Accepted 27th July 2010
DOI: 10.1039/c003770m

A solid body undergoing oscillatory motion in a fluid generates an oscillating flow. Oscillating flows in Newtonian fluids were first treated by G.G. Stokes in 1851. Since then, this problem has attracted much attention, mostly due to its technological significance. Recent advances in micro- and nanotechnology require that this problem be revisited: miniaturized mechanical resonators with linear dimensions in microns and sub-microns—microelectromechanical systems (MEMS) and nanoelectromechanical systems (NEMS), respectively—give rise to oscillating flows when operated in fluids. Yet flow parameters for these devices, such as the characteristic flow time and length scales, may deviate greatly from those in Stokes' solution. As a result, new and interesting physics emerges with important consequences to device applications. In this review, we shall provide an introduction to this area of fluid dynamics, called high-frequency nanofluidics, with emphasis on both theory and experiments.

I. Introduction

In the last few decades, we have witnessed a relentless effort to miniaturize silicon-based devices. This exciting trend, along with advances in micro and nano-fabrication techniques, has resulted in mechanical devices with micron and, more recently, sub-micron linear dimensions.[1–5] These so-called micro and nano-electro-mechanical systems (M/NEMS) are slowly finding a number of technological applications;[6–13] there is also a great deal of interest in using these devices to study fundamental physical phenomena.[14–16]

In this article, we shall limit ourselves mostly to simple mechanical resonators, such as a micro-cantilever,[5] or a doubly-clamped beam[17] or wire[18,19] as shown in Fig. 1. The mechanical resonator is typically driven by a coherent force around its (fundamental) resonance frequency, where its response is maximal. In order to measure external perturbations using the resonator, one looks for changes in the resonator's response. A ubiquitous example of resonant detection is in dynamic mode Atomic Force Microscopy (AFM):[20] the resonance frequency and linewidth of a micro-cantilever change as a result of its interaction with a probed surface, thereby providing a 'map' of the surface. Another common example is the detection of small masses.[21–25] Here, a small mass attached to a vibrating cantilever or a doubly-clamped beam results in a frequency shift proportional to the mass. Variations on this resonant detection approach are, of course, possible.[26–28]

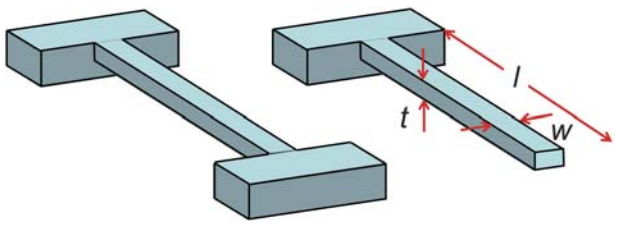

Fig. 1 Simplest commonly used M/NEMS structures. Our discussion of fluid dynamics of M/NEMS will be based on these structures. (a) A doubly-clamped beam resonator. (b) A cantilever.

The range of linear dimensions of the devices considered here span many orders of magnitude—from tens of nanometers[29] all the way up to hundreds of micrometers. As such, these devices can possess kHz to GHz[30] range frequencies with small active masses. In most measurements and applications, the energy dissipated by the resonator sets the performance limits as well as the available bandwidth.[21,31] There are several review articles,[1–5] which focus upon the device properties and applications of M/NEMS; we refer the reader to these articles for an introduction and survey. We emphasize that, with such unique properties, the possibilities for novel applications and interesting measurements[32,33] involving M/NEMS are numerous.

It is natural to consider the operation of these devices in fluids because many of the foreseeable applications, such as biochemical mass sensing, are in fluids.[34–40] The fluid dynamics of M/NEMS is therefore a technologically important problem. Conversely, M/NEMS immersed in a fluid are opening up new regimes in fluid dynamics:[41–50] the parameters in the generated flow—such as frequency, size, shear rate, and so on—are clearly pushed into unexplored regimes, where classical fluid dynamics may break down.

In this article, we present a review of the fluid dynamics of M/NEMS. Our review is intended to be instructive and starts with the simplest aspects of M/NEMS flow and builds to the most recent developments. In section II, we present a theoretical background of the problem. In section III, we describe typical experiments involving M/NEMS in fluids and discuss our universal formulation of nanoscale oscillating flows, high-frequency nanofluidics. Section IV is reserved for conclusions and outlook.

[a]*Mechanical Engineering Department, Boston University, Boston, MA, 02215, USA. E-mail: ekinci@bu.edu*
[b]*Center for Nanoscale Science and Technology, NIST, Gaithersburg, MD, 20899, USA*
[c]*Department of Chemical Engineering, Princeton University, Princeton, NJ, 08544, USA*
[d]*Holst Centre/IMEC, High Tech Campus 31, 5656, AE, Eindhoven, The Netherlands*

II. Theoretical background

The fluid dynamics of M/NEMS resonators can be formulated by simply treating the resonator as a solid body oscillating in a fluid. Through the solid-fluid boundary, an oscillating flow is set up in the fluid, which dissipates energy and results in mass loading of the resonator. A generic treatment of 'the resonator in fluid' will be given in the experimental section; in this section, we shall formulate the framework for a flow set up by an oscillating solid surface in a fluid.

II.i. Newtonian hydrodynamics

Basic concepts. A natural starting point for our discussion is the Newtonian hydrodynamics. In describing flows varying on a characteristic spatial length-scale L, Newtonian hydrodynamics is formulated in terms of a "fluid element", *i.e.*, a small volume of fluid of linear dimension $l \ll L$ containing a large number of particles, $N \gg 1$. Only in this case can one neglect the large fluctuations of macroscopic parameters, which are of order $1/\sqrt{N}$. Since $l \ll L$, all variations of flow characteristics on a scale l are negligible, and the fluid element can be treated as a mathematical point. This leads to the continuum description of fluid flow introduced by Euler in 1755. It is natural to express the length-scale l in terms of a microscopic length scale λ, generally taken as the fluid mean-free path, which is linked to the fluid density and reflects the nature of the intermolecular interactions.

The equations of hydrodynamics are expressions of conservation laws for a fluid element. The momentum conservation equation (Newton's second law) reads

$$\frac{\partial \mathbf{u}}{\partial t} + \mathbf{u}\cdot\nabla\mathbf{u} = \frac{1}{\rho}\nabla\cdot\Pi \tag{1}$$

where ρ is the mass density and $\mathbf{u}$ is the fluid velocity vector (with components u_i and magnitude u). In order for these equations to provide a closed dynamic model, the stress tensor $\Pi_{ij} = -p\delta_{ij} + \sigma_{ij}$ must be a known function of the basic hydrodynamic variables. While the spherical component $p = -\frac{1}{3}\Pi_{kk}$ can be obtained from equations of state for the thermodynamic pressure $p = p(\rho,T)$ at temperature T and/or kinematic constraints imposed by conservation of mass, there are no readily available expressions for deviatoric stresses σ_{ij} responsible for energy dissipation. In thermodynamic equilibrium with no external forces applied, the fluid is homogeneous, and thus all spatial derivatives of the fluid velocity field are zero, $\frac{\partial u_i}{\partial x_j} = 0$. In the vicinity of thermodynamic equilibrium such velocity derivatives are small and

$$\sigma_{ij} = \mu\left(\frac{\partial u_i}{\partial x_j} + \frac{\partial u_j}{\partial x_i} - \frac{2}{3}\frac{\partial u_k}{\partial x_k}\delta_{ij}\right) + \mu_b\frac{\partial u_k}{\partial x_k}\delta_{ij} + O\left(\rho\lambda^2\frac{\partial u_i}{\partial x_\alpha}\frac{\partial u_j}{\partial x_\beta}\right). \tag{2}$$

The first expansion coefficient μ is the dynamic shear viscosity, μ_b is the so-called bulk viscosity, which is zero under the Stokes' hypothesis valid for simple fluids.[51] The kinematic viscosity ν is related to μ as $\mu = \rho\nu$ (ρ is the mass density as defined above). Neglecting the high-order contributions to the expansion in eqn (2) provides the Newtonian flow approximation. In the Newtonian flow approximation, the microscopic structure of the fluid is represented by constant transport coefficients (*e.g.*, shear viscosity μ). Assuming near-equilibrium and divergence-free flow one obtains the Navier–Stokes equations for a so-called incompressible Newtonian fluid:

$$\begin{aligned}&\frac{\partial \mathbf{u}}{\partial t} + \mathbf{u}\cdot\nabla\mathbf{u} = -\frac{1}{\rho}\nabla p + \nu\nabla^2\mathbf{u},\\ &\nabla\cdot\mathbf{u} = 0.\end{aligned} \tag{3}$$

For a flow with a characteristic velocity u_0, the Reynolds number $\mathrm{Re} = \frac{u_0 L}{\nu}$ is the fundamental dimensionless parameter characterizing the flow dynamics. For typical gases, such as air, the relationship $\nu \approx \lambda c_s$ holds between the viscosity, the mean-free path and the speed of sound. Taking $c_s \approx 300$ m/s and $\nu \approx 16 \times 10^{-6}$ m^2/s, one obtains $\lambda \approx 10^{-7}$ m. In a typical dense fluid, such as water, the intermolecular separation is $\sim 5 \times 10^{-10}$ m. In this case, unlike in gases, a microscopic derivation of the relationship $\nu \approx \lambda c_s$ does not exist, but one can still apply this relationship to obtain $\lambda \approx 2 \times 10^{-9}$ m (for water, $\nu \approx 10^{-6}$ m^2/s and $c_s \approx 1500$ m/s), which corresponds to the density correlation length instead of an intermolecular separation.

Newtonian hydrodynamics of oscillating flows. We now turn to the problem of a solid object oscillating at (angular) frequency ω in a Newtonian fluid subject to the no-slip boundary condition. We first analyze the simplest case known as Stokes' second problem to establish some important physical features of the flow; we then make approximations and discuss the flow due to oscillations of an object of arbitrary shape.

Consider a Newtonian fluid filling half-space $y > 0$ in contact with a large (infinite) solid plate at $y = 0$, which moves along the x-axis with velocity $u_p = u_0\cos\omega t$. The situation is illustrated in Fig. 2a. Since the velocity components in y and z-directions are zero and effects of the edges of the large plate can be neglected, we only have to solve the equations for the x-component of the velocity field $u_x(y,t)$. Due to the symmetry of the problem we have

$$u_y = u_z = 0,\ \mathbf{u}\cdot\nabla\mathbf{u} = 0,\ \nabla\cdot\mathbf{u} = 0,\ p = \text{constant} \tag{4}$$

and the velocity field satisfies the diffusion equation,

$$\frac{\partial u_x}{\partial t} = \nu\frac{\partial^2 u_x}{\partial y^2} \tag{5}$$

which has the solution

$$u_x(y,t) = u_0 e^{-\frac{y}{\delta}}\cos\left(\omega t - \frac{y}{\delta}\right). \tag{6}$$

Here, the penetration depth (boundary layer thickness) δ emerges as the only length scale and is given by

$$\delta = \sqrt{\frac{2\nu}{\omega}}. \tag{7}$$

Two important observations can be made for Newtonian flows: the shear wave, which is dissipated on a length-scale equal to the wavelength, cannot propagate and the boundary layer becomes thinner as the frequency increases.

The energy dissipation and the fluid mass loading are the most relevant quantities for the M/NEMS experimentalist and the device expert. The force exerted on the plate by the fluid is simply

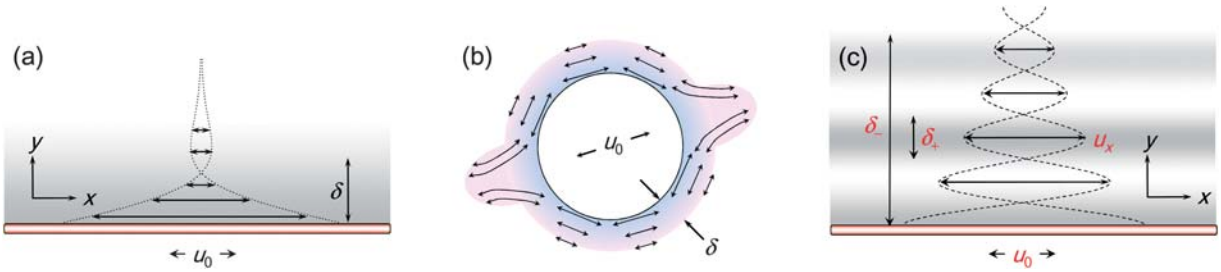

Fig. 2 Illustration of flow geometries and dynamical parameters. (a) Unsteady flow generated by an infinite plate oscillating at (angular) frequency ω with peak velocity u_0 in the Newtonian limit. The penetration depth (boundary layer thickness) is δ. (b) A body with curved surfaces oscillating at high frequency in a Newtonian fluid. Inside the boundary layer, the flow is nearly tangential to the body surface. (c)The oscillating plate problem in the non-Newtonian limit. A wavelength δ_+ and a penetration depth δ_- emerge instead of the viscous boundary layer thickness δ.

$F_x = S\mu \left.\frac{\partial u_x}{\partial y}\right|_{y=0}$ where S is the surface area of the large plate. The average energy dissipated per unit time (in units of W) is found as $\bar{\dot{E}} = \frac{Su_0{}^2}{2}\sqrt{\frac{1}{2}\rho\mu\omega}$ by averaging the dissipation rate $F_x u_p$ over the oscillation cycle. Note that, due to the symmetries mentioned above, the only dissipation comes from the so-called skin friction or Stokes friction. In general, there may also be a contribution to the dissipation from the normal stresses on the oscillating body. However, this force does not play a dominant role at high frequencies, as we show below. There is also mass loading on the plate due to the in-phase motion of the fluid. This results in a downwards shift of the resonance frequency of a M/NEMS resonator as discussed in section III.i.

Returning to eqn (3), we observe that it may be possible to linearize this equation when $|\partial\mathbf{u}/\partial t| \gg |\mathbf{u}\cdot\nabla\mathbf{u}|$ by neglecting the convection term. This relation between the derivatives corresponds to the condition $\omega u_0 \gg u_0^2/L$, where, as above, u_0 is the velocity amplitude and L is a representative linear dimension over which u_0 changes, often of the order of the linear dimensions of the oscillating body. Furthermore, in terms of the oscillation amplitude a, this condition translates into $a \ll L$ given that $u_0 = \omega a$. For high-frequency and small-amplitude oscillations of a M/NEMS resonator, this condition is typically satisfied and the linearized Navier–Stokes equation represents a valid approximation.

In the low Re limit, where the generated flow is laminar, and both turbulence and vortex shedding can be neglected, the linearized Navier–Stokes equations suggest that all oscillating flows behave in a somewhat similar way independent of geometric details. It can be shown that the fluid force acting on an arbitrarily-shaped body oscillating with velocity $u = u_0 \cos\omega t$ can be represented as a sum of two contributions,[52]

$$F = -\beta_1 u - \beta_2 \frac{du}{dt} \tag{8}$$

where the constant coefficients β_1 and β_2 contain all the relevant information about geometry, viscosity, and so on. Let us first find the energy dissipated by the oscillating object in terms of the prescribed solution in eqn (8). Similar to the oscillating plate above, the average energy dissipated per unit time can be found as $\beta_1 u_0^2/2$, which depends only upon β_1; the second term with the coefficient β_2, which is responsible for the added mass, does not contribute to the energy dissipation. To illustrate, let us consider a sphere of radius R (the result for a cylinder oscillating perpendicular to its axis is almost identical). The force can be found as

$$F = 6\pi\mu R\left(1+\frac{R}{\delta}\right)u + 3\pi R^2\sqrt{\frac{2\mu\rho}{\omega}}\left(1+\frac{2R}{9\delta}\right)\frac{du}{dt} \tag{9}$$

where the boundary layer thickness is $\delta = \sqrt{\nu/\omega}$. At low frequency, the solution becomes identical to Stokes' solution of a sphere moving in a viscous fluid. As the frequency is increased, the dissipation is completely dominated by the R/δ term; the energy dissipated per unit time converges to $6\pi R^2 u_0{}^2\sqrt{\rho\mu\omega}$. Note that the solution in eqn (9) includes the skin friction (due to viscosity) as well as the normal stress contributions. Since the flow outside the boundary layer remains inviscid, the contribution to the dissipation from the normal stress (pressure) on the body surface is zero to first order. As the frequency is increased and $R/\delta \gg 1$, this approximation becomes more and more accurate. Physically, for $\delta \ll R$, the fluid element adjacent to the solid does not feel the curvature of the solid. Hence, the oscillating body with a radius of curvature R looks increasingly similar to a plate, where normal stresses provide negligible contribution to the dissipation. This important physical concept is illustrated in Fig. 2b. We note that some authors[53] prefer to use a frequency dependent Reynolds number, $\mathrm{Re}_\omega = \frac{\omega L^2}{\nu} \approx \frac{L^2}{\delta^2}$, in order to compare δ to L ($L \sim R$ for the sphere).

In high-frequency oscillations in a Newtonian fluid, therefore, where the conditions $a \ll L$ and $\delta \ll L$ are met, the following conclusions can be drawn: The flow remains inviscid outside a small boundary layer, with typically negligible drag force from normal stresses. Inside the boundary layer, the flow is nearly tangential to the body surface, and the energy dissipation is dominated by the skin friction on the solid body. In other words, the problem becomes similar to the simple oscillating plate.

The description in eqn (9) and its consequences are valid even for more complex geometries. Fluid forces acting on two-dimensional bluff bodies undergoing periodic oscillation at angular frequency ω will exhibit similar asymptotic behavior in both limits $\mathrm{Re}_\omega \to 0$ and $\mathrm{Re}_\omega \to \infty$.[54] In order to estimate the fluid resistance to M/NEMS in Newtonian regimes, slender beam structures are conveniently modeled as cylinders that oscillate perpendicular to the axis of the cylinder. The cylinder approximation can be effectively applied for beams with a square cross-section, *i.e.*, unit aspect ratio, and empirical corrections have

been proposed for rectangular cross-section with moderate-to-large aspect ratios.[55] Similarly, mass loading can be estimated from cylinder or sphere approximations.

Limits of Newtonian hydrodynamics. A typical M/NEMS resonator in a fluid can attain a size comparable to the microscopic length scale in the fluid, especially in a rarefied gas. Similarly, the time scale of the high-frequency oscillations of the device can exceed the equilibrium relaxation time of the surrounding fluid. Consequently, application of the Newtonian approximation to the fluid dynamics of M/NEMS becomes problematic.

Considering flow past a bluff body of linear dimension L, one often assumes the characteristic length of flow variation to be $\sim L$. Given this, the very concept of a fluid element breaks down when L becomes comparable to the microscopic length scale λ of the fluid. This is traditionally expressed in terms of the Knudsen number, $\mathrm{Kn} = \lambda/L$. In other words, $\mathrm{Kn} \ll 1$ defines a natural limit for validity of the continuum approximation. Yet, kinetic theory based analysis of the breakdown of Newtonian hydrodynamics immediately reveals the ambiguity of the above criterion. Flows of complex geometry can often be characterized by different length-scales L_i, leading to multiple Knudsen numbers $\mathrm{Kn}_i = \lambda/L_i$ and, as we show below, the choice of a proper one is a nontrivial matter. Only dynamic treatment of the problem can resolve these ambiguities.

An additional criterion emerges for flows varying on a time-scale T. A fluid can be considered to relax to equilibrium in a characteristic time scale τ, called the relaxation time, when weakly perturbed. If τ becomes comparable to T, the key assumption of Newtonian hydrodynamics that the fluid remains in the vicinity of equilibrium is no longer valid. This condition is traditionally expressed in terms of the dimensionless time or the Weissenberg number, $\mathrm{Wi} \equiv \tau/T = \omega\tau \ll 1$.

In fluids, the relaxation time can be estimated *via* viscosity: $\nu \approx \tau \dfrac{k_B\theta}{m} \approx \tau {c_s}^2 \approx \lambda c_s$. Here, k_B is the Boltzmann constant, θ is the temperature and m is the molecular mass of the fluid. All other symbols have been defined above. Thus, $\tau \sim \lambda/c_s$. Given that λ stands for the mean-free path in gases, it takes a few intermolecular collisions for an initial perturbation to decay. In dense fluids the same formula can be used—albeit with λ as a characteristic correlation length of density fluctuations as noted above.

In atmospheric air at $\theta = 300$ K, $c_s \approx 300$ m/s, $\tau \approx 10^{-9}$ s and $\lambda \approx 10^{-7}$ m. For high-frequency M/NEMS resonators operating in the frequency range $\omega/2\pi \approx 1$ MHz to 1000 MHz, $10^{-2} \leq \omega\tau \leq 10$. For a typical M/NEMS characteristic length $L \approx 1$ μm, $\mathrm{Kn} \approx 0.1$. Thus, to seriously consider the limits of validity of Newtonian hydrodynamics for M/NEMS, one must deal with the interplay of two dimensionless parameters Kn and Wi.

II.ii. Kinetic theory

Basic concepts. The above discussion suggests that, in dealing with M/NEMS, one is frequently in a regime where the Navier–Stokes equations break down. One therefore needs to employ microscopic methods, such as kinetic theory, in order to capture the physics when non-equilibrium conditions prevail.

Kinetic theory describes the (microscopic) state of a physical system by means of a distribution function defined in phase space $(\mathbf{r},\mathbf{v},t)$. Such a distribution function $f(\mathbf{r},\mathbf{v},t)$ gives the number n of molecules each with mass m, within a differential volume of phase-space, with position $\mathbf{r}$ and velocity coordinate $\mathbf{v}$ at a time t. Since n actually represents a mean quantity obtained from ensemble average, $f(\mathbf{r},\mathbf{v},t)$ can thus be considered to provide a statistical description of the fluid. There are many subtle issues involving the distribution function which are beyond the scope of the discussion here; we refer the reader to in depth reviews on the topic.[56,57] Hydrodynamic variables such as the fluid density ρ and the 'hydrodynamic' velocity $\mathbf{u}$, can be obtained through the velocity moments of $f(\mathbf{r},\mathbf{v},t)$:

$$\begin{aligned} \rho(\mathbf{r},t) &= m\int f(\mathbf{r},\mathbf{v},t)d\mathbf{v}, \\ \rho\mathbf{u}(\mathbf{r},t) &= m\int f(\mathbf{r},\mathbf{v},t)\mathbf{v}d\mathbf{v}. \end{aligned} \tag{10}$$

The distribution function is governed by the Boltzmann transport equation

$$\frac{\partial f}{\partial t} + \mathbf{v}\cdot\nabla f = C(f) \tag{11}$$

indicating that, in the absence of external force fields, the evolution of $f(\mathbf{r},\mathbf{v},t)$ in the 7-dimensional phase space is determined by the translational motion of the fluid molecules and intermolecular collisions denoted by $C(f)$. Direct solution of the Boltzmann equation, in general, is quite difficult and most problems require expansion procedures or other techniques.

Relaxation time approximation. The approach here is to simplify the Boltzmann equation by replacing the collision term by a BGK ansatz, modeling relaxation to thermodynamic equilibrium.[58] In accord with Boltzmann's H-theorem, the initially perturbed non-equilibrium distribution function f monotonically relaxes to the equilibrium distribution function f^{eq} on a characteristic time scale $\tau(f)$, which is to be found from a microscopic theory. This leads to

$$\frac{\partial f}{\partial t} + \mathbf{v}\cdot\nabla f = -\frac{f - f^{eq}}{\tau}. \tag{12}$$

In the mean-field approximation, valid close to equilibrium where all gradients are small, one sets $\tau(f) = \tau =$ constant. Eqn (12) is the well-known Boltzmann-BGK (BE-BGK) equation widely used for both theoretical and numerical studies of non-equilibrium fluids.[59–61] In 3-D velocity space, the equilibrium distribution is $f^{eq} = \dfrac{n}{(2\pi k_B\theta/m)^{3/2}}\exp\left(-\dfrac{m(\mathbf{v}-\mathbf{u})^2}{2k_B\theta}\right)$ with $n = \rho/m$ and $\theta = \dfrac{m}{3nk_B}\displaystyle\int f(\mathbf{v}-\mathbf{u})^2 d\mathbf{v}$. We stress that the BE-BGK equation is not the outcome of a systematic procedure applied to Hamiltonian equations of motion or Boltzmann transport equations. Rather, BE-BGK constitutes a phenomenological model satisfying basic conservation laws and symmetries of the problem. In the limit of $\mathrm{Kn} \ll 1$ and $\mathrm{Wi} \ll 1$, BE-BGK leads to the Navier–Stokes equations, thus justifying its validity for Newtonian flows. At the present time, the applicability of BE-BGK in strongly non-equilibrium flows can only be determined by comparison with experiments.

In order to obtain the momentum conservation equation, one takes the first velocity moment of the BE-BGK to obtain

$$\frac{\partial \mathbf{u}}{\partial t} + \mathbf{u}\cdot\nabla\mathbf{u} = \frac{1}{\rho}\nabla\cdot\Pi \tag{13}$$

where the stress tensor is

$$\Pi_{ij} = -p\delta_{ij} + \sigma_{ij} = -m\int f(v_i - u_i)(v_j - u_j)d\mathbf{v} \tag{14}$$

To close eqn (13), one attempts to evaluate the stress tensor as a functional of basic hydrodynamic variables (*e.g.*, ρ and $\mathbf{u}$). If relaxation to equilibrium is very rapid, *i.e.*, $\tau \to 0$, the left-hand side of eqn (12) becomes negligible and thus $f \approx f^{eq}$; the zeroth-order approximation $f = f^{eq}$ gives $\Pi_{ij} = -p\delta_{ij} = -nk_B\theta\delta_{ij}$ and $\sigma = 0$. The situation is quite different in non-equilibrium. To find a solution to the kinetic equation one can resort to a perturbation expansion $f = f^{eq} + \varepsilon f^{(1)} + \varepsilon^2 f^{(2)} + \ldots$ in powers of small dimensionless parameters ε. This procedure was first developed for the Boltzmann equation by Chapman and Enskog.[62,63] In the second-order of the so-called Chapman-Enskog (C–E) expansion one derives[64]

$$\sigma_{ij} \approx \sigma_{ij}^{(1)} + \sigma_{ij}^{(2)} = \overbrace{2\mu S_{ij}}^{first-order}$$

$$\overbrace{-2\mu\tau\left[\frac{D}{Dt}S_{ij} + 2\left(S_{ik}S_{kj} - \frac{1}{3}S_{kl}S_{kl}\delta_{ij}\right) - \left(S_{ik}\Omega_{kj} + S_{jk}\Omega_{ki}\right)\right]}^{second-order} \tag{15}$$

in the incompressible flow limit ($\nabla\cdot\mathbf{u} = 0$). Here, the rate-of-strain and vorticity tensors are defined as $S_{ij} = \frac{1}{2}\left(\frac{\partial u_i}{\partial x_j} + \frac{\partial u_j}{\partial x_i}\right)$ and $\Omega_{ij} = \frac{1}{2}\left(\frac{\partial u_i}{\partial x_j} - \frac{\partial u_j}{\partial x_i}\right)$ respectively, the dynamic viscosity is $\mu = \rho\tau\theta$, and $\frac{D}{Dt} \equiv \left(\frac{\partial}{\partial t} + \mathbf{u}\cdot\nabla\right)$. The first term in the right side of eqn (15), given by the first-order C–E expansion, corresponds to the Newtonian fluid approximation [eqn (2)]. Meanwhile, nonlinear (non–Newtonian) corrections, expressed by the remaining terms in eqn (15), are generated in the second-order expansion. The second-order constitutive relation (15) is quite complex and, in general, can be only attacked by numerical methods. For the general case, complexity of the high-order contributions coming from proliferation of tensorial indices makes derivation of high-order corrections to hydrodynamic approximations extremely difficult, if not impossible.

High-frequency limit of oscillating flows. We now turn to oscillating flows in the high frequency limit. The equation for the velocity field can be derived from the BE-BGK for the simple but physically relevant case of Stokes' second problem. The derivation is provided in the Appendix. The equation governing the flow is the so-called "telegrapher's equation":

$$\frac{\partial^2 u}{\partial t^2} + \frac{1}{\tau}\frac{\partial u}{\partial t} = c_s^2\frac{\partial^2 u}{\partial y^2}. \tag{16}$$

The solution to this equation subject to boundary conditions $u(y = 0) = u_0$ and $u(y \to \infty) = 0$ is

$$u = u_0 e^{-\frac{y}{\delta_-}}\cos\left(\omega t - \frac{y}{\delta_+}\right) \tag{17}$$

with

$$\frac{1}{\delta_\pm} = \left(1 + \omega^2\tau^2\right)^{\frac{1}{4}}\sqrt{\frac{\omega}{2\nu}}\left[\cos\left(\frac{\tan^{-1}\omega\tau}{2}\right) \pm \sin\left(\frac{\tan^{-1}\omega\tau}{2}\right)\right]. \tag{18}$$

Accordingly, the energy dissipation rate can be calculated as

$$\bar{\dot{E}}(\tau,\omega) = \frac{S\mu {u_0}^2}{2(1+\omega^2\tau^2)}\left(\frac{1}{\delta_-} + \frac{\omega\tau}{\delta_+}\right). \tag{19}$$

Let us now turn to the implications of the above solution. First, all the quantities above converge to their Newtonian values as $\tau \to 0$; this is the basic property of a Newtonian fluid. Note also that all the quantities are symmetric in τ and ω with the exception of the Newtonian boundary layer thickness $\delta = \sqrt{\frac{2\nu}{\omega}}$. It therefore makes sense to refer to the limit $\omega\tau \to 0$ as the Newtonian limit. As $\omega\tau \to 0$, the penetration depth and the wavelength become equal, $\delta_-/\delta_+ \to 1$. In the high-frequency non-Newtonian limit $\omega\tau \to \infty$, the penetration depth saturates, $\delta_- \to 2\lambda$, but $\delta_+ \to \lambda/\omega\tau \to 0$, so that the ratio $\delta_-/\delta_+ \to \omega\tau$. This result defines a propagating shear wave in the boundary layer ($\delta_- \approx \lambda$). Fig. 3 displays the main parameters of high-frequency oscillating flows.

Hydrodynamic boundary conditions. An important issue in finite Weissenberg or Knudsen number flows is the determination of proper boundary conditions for the solution of eqn (16). Such hydrodynamic (coarse-grained) boundary conditions are determined by complex interactions at microscopic level. According to the classic depiction of slip at a solid wall due to Maxwell, a finite mean-free-path λ and rate-of-strain at the solid-fluid interface produce an effective slip velocity

$$u_s = u(y = 0) - u_0 = \alpha\lambda\left.\frac{\partial u}{\partial y}\right|_{y=0} + \mathrm{O}\left(\lambda^2\left.\frac{\partial^2 u}{\partial y^2}\right|_{y=0}\right). \tag{20}$$

Here, $u(y = 0)$ is the tangential component of the fluid velocity at the wall, u_0 is the actual wall velocity, y is the wall-normal direction (pointing into the fluid bulk), and α is a slip coefficient. In the case of steady isothermal flows, the slip coefficient $\alpha = \frac{2 - \sigma_v}{\sigma_v}$ is determined by the so-called surface accommodation parameter σ_v that ranges between 0 (specular reflection) and 1 (diffuse scattering) for isothermal and perfectly elastic surfaces. In studies dealing with unsteady flows, different surface roughness, and wetting properties, widely diverse slip velocities have been observed *via* experimental and numerical methods.[65] For near-equilibrium flows where $\lambda^n\left|\frac{\partial^n u}{\partial y^n}\right| \ll 1$ ($n \geq 1$), the classic no-slip boundary condition $u(y = 0) = u_0$ has proven to be an accurate approximation. On the other hand, for complex flows in far-from-equilibrium conditions the applicability of effective slip models has not been fully elucidated.

It is worth notice that in the studied oscillating flows, the governing hydrodynamic equations are linear and thus general boundary conditions can be easily introduced into or factored out of the flow solution by linear scaling: a fluid velocity $u(y = 0) = u_0 + u_s$ can be adopted in lieu of $u(y = 0) = u_0$ in eqn (17) and thereafter.

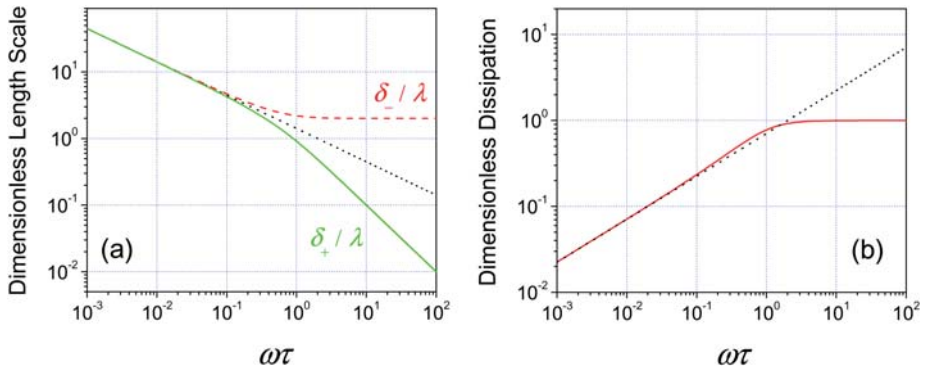

Fig. 3 Length scales and energy dissipation in high-frequency oscillating flows as a function of dimensionless frequency $\omega\tau$. (a) The solid line is the wavelength δ_+/λ. The dashed line is the penetration depth δ_-/λ. The dotted line shows the boundary layer thickness in Newtonian fluid. (b) Dimensionless energy dissipation $\frac{\overline{\dot{E}}(\tau,\omega)}{\frac{1}{2}S\rho u_0{}^2 c_s}$ as a function of $\omega\tau$ for both the Newtonian (dotted line) and the high-frequency solutions.

Numerical simulation. In addition to analytical methods, numerical simulations are commonly employed to study complex flows. A number of different approaches,[49] such as the lattice Boltzmann method (LBM), direct simulation Monte Carlo (DSMC) and so on, have been applied to flows involving M/NEMS. While LBM is based on numerical solution of BE-BGK, the standard DSMC approach mimics a microscopic dynamics governed by the classic Boltzmann equation with binary interparticle collisions. It has been established that both LBM and DSMC approaches simulate the Navier–Stokes hydrodynamics for general flows in near-equilibrium conditions (Kn $\rightarrow$ 0, $\omega\tau \rightarrow 0$). Furthermore, recent studies[66] present comparable results for steady flows over a wide range of Knudsen number well within transitional regimes. In the case of oscillating flows, substantially different flow dynamics are predicted for the high-frequency limit $\omega\tau \gg 1$, even though both approaches report comparable fluidic damping. For $\omega\tau \rightarrow \infty$, while LBM and approximations based on BE-BGK introduce memory effects responsible for elastic fluid response in the bulk, DSMC simulations have been favorably compared against analytical solutions for free-molecular flow. Recent work[67] has demonstrated that LBM approaches based on Galerkin projection of the BE-BGK can accurately predict fluidic effects on different M/NEMS oscillators experimentally measured in a wide range of operation conditions.

II.iii. Scaling

Formulating a type of flow in terms of proper dimensionless numbers and extracting scaling behavior is a powerful approach to fluid dynamics. Proper dimensionless numbers form a natural system of units and determine the physical characteristics of the flow uniquely. For instance, for a *steady* Newtonian flow past a solid body, the Reynolds number $\mathrm{Re} = \frac{u_0 L}{\nu}$ emerges as the only relevant parameter from the Navier–Stokes equations. Here, as above, u_0 is a characteristic velocity; L is a characteristic length scale, typically, of order of the linear dimensions of the body, and ν is the kinematic viscosity. In other words, the particular details of the flow are all embedded in Re. Thus, data obtained in different experiments—for instance, on drag coefficients—can conveniently be collapsed onto a single curve as a function of Re. It is also due to this scaling law that an engineer can accurately predict flow in full-scale designs by making measurements on scaled-down models.

The simple and elegant scaling behavior of steady flows quickly becomes complicated as one ventures into flows where deviations from equilibrium are no longer small and higher-order stress terms in the series $\sigma_{ij} \approx \sigma_{ij}^{(1)} + \sigma_{ij}^{(2)} + \ldots$ become relevant [see eqn (2)]. The series, in general, can be considered an expansion in terms of space and time derivatives. It is thus possible to cast the solution into an expansion in terms of Kn and Wi through proper non-dimensionalization.

We now turn to the scaling behavior of high-frequency oscillating flows. The dimensionless time in this problem is given by $\mathrm{Wi} = \tau/T = \omega\tau$, as mentioned above. At the Newtonian limit of Stokes' second problem, the only length scale available is $\delta \approx \sqrt{\frac{\nu}{\omega}} \sim \frac{\lambda}{\sqrt{\omega\tau}}$, leading to a Knudsen number, $\mathrm{Kn}_\delta \approx \sqrt{\omega\tau}$ (we henceforth differentiate between various Knudsen numbers by using a subscript). This Knudsen number must remain small ($\omega\tau \ll 1$) since $\omega\tau \geq 1$ ($\lambda > \delta$) corresponds to an unphysical situation. This is because intermolecular collisions must create the boundary layer. This argument shows that the validity of the Newtonian approximation is indeed determined by the condition $\omega\tau \ll 1$. At the high-frequency limit, the solution provided above in eqn (17)–(18) from kinetic theory can be used to determine the scaling behavior. Forming dimensionless groups for the parameters of this solution, we obtain the following: $\mathrm{Kn}_{\delta_-} = \frac{\lambda}{\delta_-} \rightarrow \frac{1}{2}$ and $\mathrm{Kn}_{\delta_+} = \frac{\lambda}{\delta_+} \rightarrow \omega\tau$ as $\omega\tau \rightarrow \infty$. The first Knudsen number, Kn_{δ_-}, cannot serve as a scaling parameter since it does not cover the possible range of values. The second Knudsen number, Kn_{δ_+}, thus emerges as the desired scaling parameter and furthermore, $\mathrm{Kn}_{\delta_+} = \mathrm{Wi}$ for high-frequency oscillating flows.

Previous attempts to characterize flows involving M/NEMS resonators employed a geometric dimension w as characteristic flow length rather than following the kinetic arguments described above. In one approach,[45] a Knudsen number $\mathrm{Kn}_w = \lambda/w$ (see Fig. 1) is taken as a scaling parameter. When $\mathrm{Kn}_w \ll 1$, the flow is described by classical Newtonian solutions. In the region

$\mathrm{Kn}_w \gg 1$, a kinetic treatment, accounting only for collisions between the resonator and gas particles (*i.e.*, free-molecular flow approximation) is used for determining the forces acting on the oscillating body. This approach, however, did not provide reasonable predictions in the transitional regime $\mathrm{Kn}_w \sim 1$. In other work,[68,69] the focus has been on understanding the squeezing or lubrication flow produced in various N/MEMS applications, where there is a narrow gap between the resonator and a stationary substrate. In the transitional regime, this type of flow has been commonly treated by applying diverse slip boundary conditions in an attempt to account for rarefaction and other kinetic effects, which are always present within the Knudsen layer adjacent to the fluid-solid interface. This approach has provided predictions for the fluidic damping for steady flows of rarefied gases. The solutions come in the form of expansions in terms of Kn_w with w given by the gap size.[68,69]

It is important to note that one is typically interested in macroscopic parameters (observable quantities) determined by a large number of microscopic interactions, *e.g.*, collisions between the resonator and fluid molecules. Thus, one is after the governing hydrodynamic equations that determine the evolution of macroscopic variables. In order to model the effect of microscopic interactions, macroscopic conservation equations typically resort to constitutive relations. A well-known example of a linear constitutive relation is the Newtonian fluid approximation [eqn (2)], which involves constant transport coefficients (shear viscosity) and first-order spatial derivatives of the fluid momentum. In the case of steady flows when $\mathrm{Kn} \sim 1$, rarefaction effects cause spatial fluctuations in macroscopic parameters and one consequently must resort to higher-order derivatives of hydrodynamic variables resulting in nonlinear relations. For high-frequency oscillating flows and $\mathrm{Wi} \sim 1$, however, deviations from Newtonian hydrodynamics are predominantly caused by nonlinearities (*e.g.*, timespace dependence of transport coefficients) arising when macroscopic quantities vary on time scales of-the-order of the relaxation time of the fluid.

III. Experiments

III.i. Damped harmonic oscillator model of a M/NEMS resonator

An elastic structure can be approximated as a damped harmonic oscillator around its resonant modes, if the resonances are well-separated.[70] The structure moves at a single frequency, modeled as a lumped mass m_i attached to a spring of stiffness k_i. The position of the mass in one-dimensional oscillatory motion is described by coordinate x. In the absence of a surrounding fluid (*i.e.*, in vacuum), the equation of motion of the one-dimensional oscillator reads:

$$x_{tt} + \gamma_i x_t + \omega_i^2 x = R(t)/m_i. \tag{21}$$

Here, x_t denotes the time derivative of x, $R(t)$ is an external drive force; γ_i accounts for the intrinsic energy dissipation; ω_i is the resonance frequency and $\omega_i = \sqrt{k_i/m_i}$. A quality factor can be defined as $Q_i \equiv \frac{\omega_i E_{st}}{\bar{\dot{E}}} = \frac{\omega_i}{\gamma_i}$; E_{st} is the energy stored in the oscillations of the resonator. Note that the subscript i stands for intrinsic in all the above quantities.

We are interested in determining the increase in the dissipation and the effective resonator mass due to the fluid. First, we consider the case of a Newtonian fluid. Rewriting the fluid force on the oscillating resonator, described in eqn (21), as $-m_i\gamma_f u - m_i\beta_f \frac{du}{dt}$, we obtain

$$(1 + \beta_f)x_{tt} + (\gamma_i + \gamma_f)x_t + \omega_i^2 x = R(t)/m_i. \tag{22}$$

The fluid thus generates a contribution to both the oscillatory mass and the dissipation. The loaded parameters of the oscillator are $\omega_L \approx \omega_i\sqrt{\frac{1}{1+\beta_f}}$ and $\gamma_L \approx \gamma_i + \gamma_f$. In a dense fluid such as water, a M/NEMS resonator typically satisfies $\gamma_L \approx \gamma_f$ since $\gamma_i \ll \gamma_f$. As such, structural dissipation can be neglected and the loaded quality factor Q_L is determined by the fluidic dissipation $\frac{1}{Q_f}, \frac{1}{Q_L} \approx \frac{1}{Q_f} \approx \frac{\gamma_f}{\omega_L}$. On the other hand in a rarified gas, $\beta_f \ll 1$ and $\frac{1}{Q_L} \approx \frac{1}{Q_i} + \frac{1}{Q_f}$.

In a typical experiment, harmonic motion of a M/NEMS resonator can be actuated by electrostatic,[71] photothermal,[72] or inertial forces.[73] One usually measures the response of the M/NEMS resonator as a function of the frequency of the actuation force near a resonance under different environmental (fluidic) conditions,[41,42] again using optical[74–78] and electrical[79] techniques. It follows from eqn (22) that the frequency response is in the form of a Lorentzian, which provides the resonance frequency and the Q as a function of the fluid loading. Alternatively, the drive force can be removed altogether and just the thermal fluctuations of the resonator can be measured in any one of its resonant modes. Curve fitting again provides the resonance frequency and the Q. In all the measurements, it is important to keep the resonance amplitudes of the resonators extremely small, within the linear limit. In Fig. 4, the driven frequency response of a nanomechanical beam resonator around its fundamental out-of-plane resonance is shown in nitrogen (N_2) at different pressures. The normalized frequency ω/ω_0 and Q as a function of pressure are plotted in Fig. 4(b) and (c), respectively. Both the frequency and the Q saturate as the pressure is lowered, converging to their intrinsic values.

III.ii. Results

The above discussion on resonators and the theoretical framework provided in section II can now be applied to experiments on high-frequency flows. An ideal system to study high-frequency nanofluidics is a simple, relatively inert gas, such as N_2. The ideal gas law provides a good approximation for the macroscopic parameters of the gas: The viscosity μ is independent of the pressure p and the relaxation time can be expressed as $\tau = \mu/p$. Thus, by changing the gas pressure and the resonator frequency, one can explore a broad range of $\omega\tau$. Moreover, the fact that $\lambda \propto 1/p$ provides an accurate way to test the effects of Kn on the flow.

The theory provides the average energy dissipated, $\bar{\dot{E}}$, *i.e.*, eqn (19) (in units of W), for a large plate. In order to make further

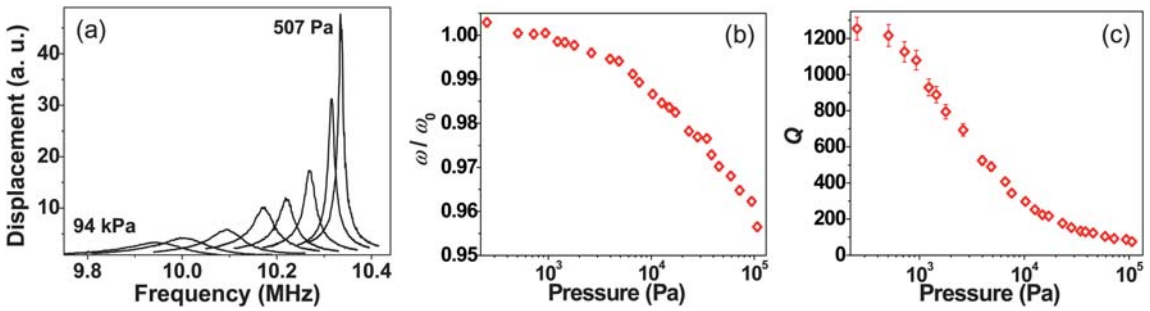

Fig. 4 (a) Fundamental resonance of a silicon doubly clamped beam of width $w = 500$ nm, thickness $t = 280$ nm, and length $l = 17.1$ μm at various dry nitrogen pressures: $p = 0.507$, 4.84, 7.59, 12.6, 28.1 and 94 kPa. (b) The normalized resonance frequency and (c) Q of the same device as a function of pressure. Notice that the fluidic dissipation becomes appreciable around 10^3 Pa and the crossover from non-Newtonian to Newtonian flow ($\omega\tau \approx 1$) takes place around 10^4 Pa. The error bars in the data arise due to thermal fluctuations in resonance, measurement noise and fitting errors. For most data points, they are smaller than the symbol size.

progress, we approximate the M/NEMS resonator as a plate with surface area (wet area) S. The motivation for the assumption comes from the fact that the high frequency flow becomes tangential to the surface as discussed in section II; any object oscillating in a fluid at high frequencies can thus be described as a plate to a good approximation. Fluidic energy dissipation can be related to quality factor as $\frac{1}{Q_f} = \frac{\bar{E}}{\omega E_{st}}$, where $E_{st} \approx \frac{1}{2} m_i {u_0}^2$ is the energy stored in the resonator. Using the average dissipated energy from eqn (19) and rearranging terms, we arrive at the expression

$$\frac{1}{Q_f} \approx \frac{S}{m} f(\omega\tau)\sqrt{\frac{\mu\rho}{2\omega}}. \tag{23}$$

The index i referring to intrinsic values has been dropped for brevity. All the symbols have been defined in eqn (23) with the exception of $f(\omega\tau)$ [not to be confused with the distribution function $f(\mathbf{r},\mathbf{v},t)$ above], which is a dimensionless function obtained from eqn (18) and eqn (19),

$$f(\omega\tau) = \frac{1}{(1+\omega^2\tau^2)^{3/4}}\left[(1+\omega\tau)\cos\left(\frac{\tan^{-1}\omega\tau}{2}\right) - (1-\omega\tau)\sin\left(\frac{\tan^{-1}\omega\tau}{2}\right)\right]. \tag{24}$$

Fig. 5 shows $\frac{1}{Q_f}$ for a number of resonators with different sizes and shapes as a function of pressure. The solid lines are self-consistent fits to data based on eqn (24), where all parameters except for τ are available. In order to obtain the fits, we assume that τ satisfies the empirical ideal gas form $\tau \propto 1/p$. In the bulk of the gas, the proportionality constant is the viscosity, $\tau = \mu/p$. This value, however, only reflects interactions between gas molecules; in the experiments, however, gas-solid surface interactions determine the proportionality constant. In order to account for this, we extracted the proportionality constant from experimental data as follows: At $\omega\tau \approx 1$, all the experimental data show a change in slope, transitioning from $\frac{1}{Q_f} \propto p$

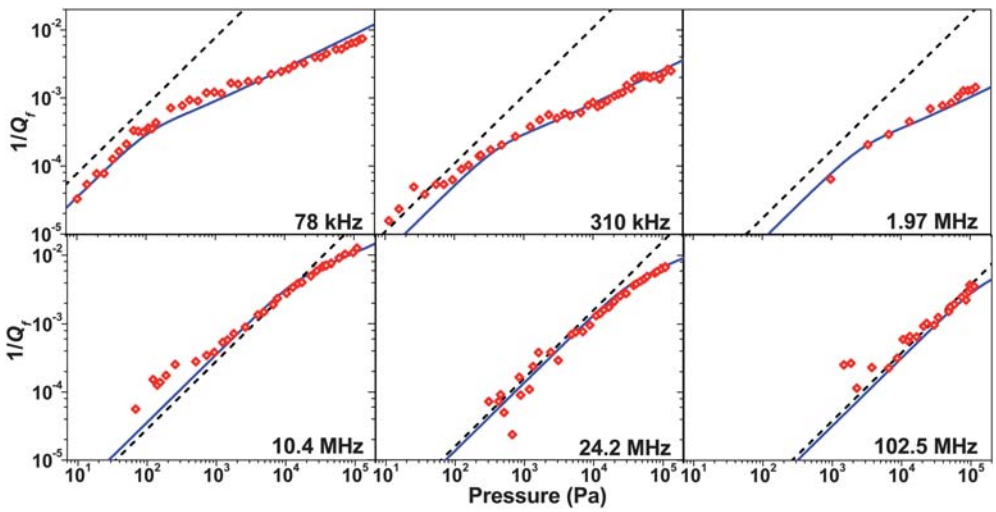

Fig. 5 Fluidic dissipation $1/Q_f$ as a function of pressure for cantilevers (top row) and doubly-clamped beams (bottom) with varying linear dimensions.[41] The dashed lines are fits to the molecular collision model.[45] High-frequency nanofluidics predictions are the solid lines calculated from eqn (24) using $\tau \approx$ (246 μs-Pa)/p. The molecular collision and the high-frequency nanofluidics predictions were multiplied by fitting constants of order 1.

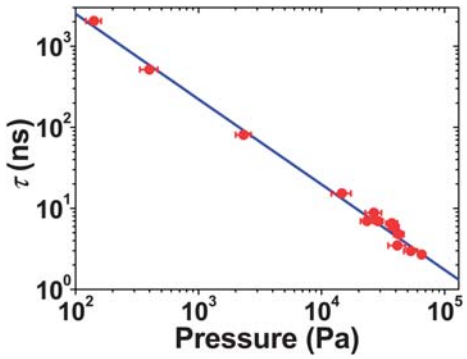

Fig. 6 Pressure dependence of the relaxation time τ, extracted from the transition point $\omega\tau \approx 1$ (crossover from non-Newtonian to Newtonian flow) observed in the dissipation data sets of many resonators, such as those shown in Fig. 4 and 5.[41] Best fit line provides the empirical correlation $\tau \approx (246 \pm 30\ \mu\text{s-Pa})/p$.

(non-Newtonian or molecular flow) to $\frac{1}{Q_f} \propto p^{1/2}$ (Newtonian or viscous flow). Given the resonator frequency ω and the transition pressure, τ can be extracted as a function of pressure as shown in Fig. 6, yielding the empirical relation $\tau \approx \frac{246 \pm 30}{p}\ \mu$s-Pa ($p$ is in units of Pa). The end result of this exercise is the self-consistent fits in Fig. 5. To improve the fits, the results emerging from eqn (24) were multiplied by fitting factors of order 1.

The above discussion establishes the role $\omega\tau$ plays in high-frequency nanofluidics of M/NEMS resonators. In a complimentary set of experiments,[42] we have looked for size effects in high-frequency nanofluidics, *i.e.*, possible scaling behavior based upon Kn. In order to do this, we extended our measurements to macroscopic quartz resonators. In thickness shear mode, the flow for small amplitude oscillations of quartz resonators matches the flow generated by a large plate to a very good approximation. In Fig. 7, we compare $1/Q_f$ data on resonators, which span a broad range of linear dimension L, oscillate in different modes (illustrated in the insets) but at close frequencies: a macroscopic quartz crystal in shear mode at 5 MHz; a microcantilever and a nanomechanical doubly-clamped beam in flexural modes at 1.97 and 24.2 MHz. Here, the dynamically relevant linear dimension of the flow is taken as $L \approx S^{1/2}$, determined by the surface area of the resonator. For the quartz crystal $L_Q \approx 10^{-2}$m, for the cantilever $L_C \approx 10^{-4}$m and for the beam $L_B \approx 3 \times 10^{-6}$m. The Knudsen numbers $\text{Kn} = \lambda/L$ for the devices are shown on the upper axes. Two observations are noteworthy: the dissipative behaviors are similar for all vibration modes, and the L or Kn appears to have no effect on the flow. These measurements establish that the simple size dependent Kn is not a relevant parameter for small amplitude high-frequency flows—as long as the oscillating body has one macroscopic dimension and, subsequently, a macroscopic number of collisions with the fluid. Furthermore, the shape and oscillation-mode independence of the data provide indirect support for the assumption that the flow remains tangential to the solid surface and skin friction dominates the dissipation. If the opposite were true, the same approach would not be able to provide acceptable fits to large plates as well as slender beams and cantilevers.

IV. Scaling and universality

The data obtained from different resonators can be collapsed onto a dimensionless plot as shown in Fig. 8. Here, the dimensionless function $f(\omega\tau)$ of eqn (24) is plotted against the dimensionless Weissenberg number $\text{Wi} = \omega\tau$. Each symbol in the plot represents a separate device with parameters displayed in Table 1. The collapsed data were obtained as follows: Using eqn (23), $1/Q_f$ values for each device were scaled to obtain f as a function of pressure; the pressure axis for each resonator was subsequently converted into $\omega\tau$ by using the empirical relationship $\tau \approx \frac{246 \pm 30}{p}\ \mu$s-Pa ($p$ is in units of Pa) along with the resonator frequency ω. The solid line is $f(\omega\tau)$ calculated from eqn (24). In analyzing the data of flexural resonators, a fitting factor of 2.8 was used as opposed to the near unity fitting factors used for the shear-mode quartz crystals.

There are two distinct regimes in the data: the viscous (Newtonian) regime as $\omega\tau \rightarrow 0$ and the opposite limit of high-frequency (non-Newtonian) flow. All the data from different resonators, with length scales extending from sub-microns all the way up to millimeters, follow the same trends. Moreover, the shape of the resonator and the way it oscillates (mode) does not

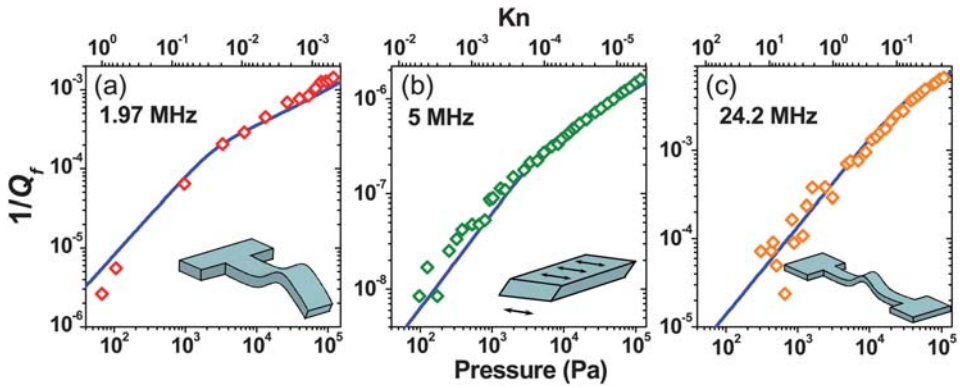

Fig. 7 Pressure dependent fluidic dissipation across length scales, measured using (a) a microcantilever with linear dimensions ($l \times w \times t$) 125 μm × 36 μm × 3.6 μm resonating in its first flexural harmonic mode in the out-of-plane direction, (b) a quartz crystal of diameter 0.5 cm and thickness ~0.1 mm moving in fundamental shear mode. (c) A nanomechanical doubly-clamped beam with linear dimensions ($l \times w \times t$) 9.6 μm × 0.23 μm × 0.2 μm moving in fundamental out-of-plane flexural mode. The upper axes shows $\text{Kn} = \lambda/L$. Solid lines are fits to eqn (24) using $\tau \approx (246\ \mu\text{s-Pa})/p$.

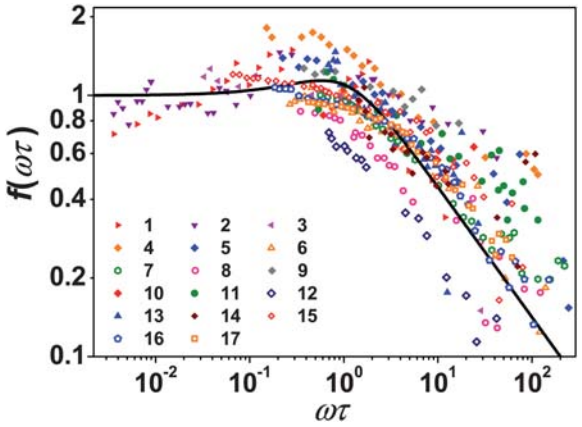

Fig. 8 Scaling of fluidic dissipation obtained from quartz resonators, microcantilevers and nanomechanical beams. Fitting factors of order one and *S*/*m* values calculated from geometry and mode shape were used.[41] The solid line is the dimensionless dissipation function $f(\omega\tau)$ of eqn (24).

Table 1 The parameters for devices of Fig. 8. The letters c, b and q stand for cantilever, doubly-clamped beam and quartz, respectively. The linear dimensions for the beams and cantilevers are as shown in Fig. 1. These are typically operated in flexural modes. The quartz crystals are in the form of thin disks with diameter ~1 cm and varying thicknesses ~0.1 mm. They are operated in thickness shear modes

No.	Type	$w \times t \times L$ (μm)	f_0 (MHz)
1	c	53 × 2 × 460	0.078 (1st Harmonic)
2	c	36 × 3.6 × 125	0.31 (fundamental
3	c	36 × 3.6 × 125	1.97 (1st Harmonic)
4	b	0.50 × 0.28 × 17.1	10.4
5	b	0.50 × 0.28 × 11.2	18.1
6	b	0.93 × 0.22 × 9.9	22.8
7	b	0.76 × 0.22 × 9.9	22.9
8	b	0.23 × 0.20 × 9.6	24.2
9	b	0.50 × 0.28 × 9.1	27.1
10	b	0.32 × 0.20 × 7.7	33.2
11	b	0.50 × 0.28 × 5.9	45.7
12	b	0.25 × 0.20 × 5.6	53.2
13	b	0.73 × 0.23 × 5.6	58.6
14	b	0.24 × 0.20 × 3.6	102.5
15	q	—	5
16	q	—	14.3
17	q	—	32.7

seem to have a strong effect on the flow as long as the amplitude of oscillation is small. The only relevant parameter, which determines the flow is $\mathrm{Wi} = \omega\tau$. In other words, all characteristics of the flow, including the constitutive stress-strain relations, the flow geometry, size and so on, are embedded in the single parameter $\mathrm{Wi} = \omega\tau$; such behavior in physical systems is typically considered a universality.

Recent experiments of Svitelskiy *et al.*[44] have extended the parameter space of this universality and shed more light on high-frequency nanofluidics. Their data show general agreement with the theoretical development and the experimental data presented here for $0.1 < \omega\tau < \infty$ for a number of different gases including CO_2, N_2 and He. Svitelskiy *et al.*, however, show that in the viscous regime, the simple plate solution becomes less and less accurate. They suggest that this effect may simply be due to mass loading. Furthermore, these authors present a different explanation for the deviation of the experimentally determined relaxation time from that in bulk. They suggest that many intermolecular collisions may be needed to establish equilibrium, thereby leading to a longer relaxation time.

V. Conclusions and outlook

We have presented a universal formulation of the fluid dynamics of M/NEMS resonators. In this formulation, the fluid relaxation time τ in conjunction with the resonator frequency ω determines the nature of the flow; linear dimension and geometry appear to have weak effects. As $\omega\tau \ll 1$, the Newtonian approximation provides accurate predictions of the flow generated by M/NEMS resonators; this is typically referred to as the viscous or the Newtonian limit. At $\omega\tau \sim 1$, the flow starts to deviate from the Newtonian approximation, and as $\omega\tau \gg 1$, viscoelastic and eventually ($\omega\tau \to \infty$) elastic fluid response emerges. This is the non-Newtonian or high-frequency flow regime. Here, the invalidity of the Newtonian approximation for $\omega\tau > 1$ is not only due to surface effects, which might be absorbed by proper hydrodynamic boundary conditions, but also due to the qualitatively different fluid dynamics in the bulk: the simple linear relation between stress and rate-of-strain in a Newtonian fluid breaks down at high frequencies. Such viscoelastic response of simple fluids (gases) in the high-frequency limit is a well-known phenomenon within the realm of transport theory and statistical physics:[80] diffusion processes in non-equilibrium systems can only be established after a finite time of the order of the relaxation time τ. When one looks at the fluid for a short time compared to its relaxation time, where diffusion effects are still weak and transport coefficients such as shear viscosity become frequency dependent, one observes an ensuing decay in the dissipation of fluid momentum and energy.

In our experiments, $\mathrm{Re} \sim 0$ and nonlinear effects, such as hydrodynamic instabilities and viscoelastic turbulence, are not present.[81] The observed transition is due to the intrinsic dynamical response of the simple fluid to high-frequency perturbations. Similar observations are commonplace in macroscopic flows of concentrated long-chain polymer solutions, where τ can be long and, consequently, $\omega\tau > 1$ due to the relatively slow polymer dynamics.[82–84] In rheology, polymers are often treated as elastic springs, and viscoelastic behavior of polymer solutions is attributed to the direct contribution of polymer molecules to the stress tensor. In kinetic theory, the breakdown of the Navier–Stokes equations for $\mathrm{Kn} \sim 1$ and/or $\mathrm{Wi} \sim 1$ is usually attributed to ballistic dynamics or kinetic effects associated with the relatively low frequency of inter-particle collisions. Kinetic equations predict that inertial forces become dominant in the high-frequency limit while viscous terms vanish in the hydrodynamic limit. The 'viscoelastic' response observed here at $\omega\tau > 1$ is linked to the underlying microscopic dynamics, *i.e.*, kinetic and 'viscoelastic' effects correspond to the same phenomenon in the studied systems. In this sense, our work points to a deep dynamical connection between oscillating flows of complex and simple fluids.

Finally, there is a relentless effort to develop M/NEMS resonators operating in gaseous[85] and liquid environments.[86] As noted above the dissipation or the Q sets the performance limits of a M/NEMS resonator. In mass sensing, for instance, a large

resonator Q translates directly into high mass resolution. The fluid dynamics discussed here should impact the design of next generation M/NEMS resonators. First, it is important to observe that shrinking the size of a resonator (M/NEMS) tends to put one at a disadvantage in fluids: as a resonator is shrunk in size, its surface-to-volume ratio gets larger; fluidic dissipation should scale with the surface area, while stored mechanical energy should be proportional to the resonator volume. The prefactor S/m in eqn (23) is a manifestation of this fact. Second, the theory and the data in Fig. 8 suggest that $f(\omega\tau)$, which determines the dissipation in fluid or Q_f [see eqn (23)] is a decreasing function of $\omega\tau$ as $\omega\tau$ grows beyond $\omega\tau > 1$. Given two resonators with identical S/m ratios, the higher-frequency resonator will always be more resilient in a given fluid, but the degree of resilience depends upon the fluid τ and the value of $f(\omega\tau)$. In this sense, the function $f(\omega\tau)$ can be used as a design aid. It may also be feasible to decrease the effective relaxation time of the fluid through less trivial mechanisms, *e.g.* through polymer addition or foams for water. Other strategies that can potentially improve device performance include modifying the cross-sectional shape and surface properties. The employment of hydrophobic or super-hydrophobic coatings for resonators in water could further increase the effective hydrodynamic slip with a subsequent reduction of the resistance forces.

Appendix 1. Derivation of telegrapher's equation

Extended hydrodynamics from BE-BGK

The BE-BGK [eqn (12)], having a linear advection term, can be solved by integrating along the characteristics

$$f(\mathbf{r},\mathbf{v},t) = \int_0^{t/\tau} e^{-s} f^{eq}(\mathbf{r}-\mathbf{v}\tau s,\mathbf{v},t-\tau s)ds + f_0(\mathbf{r}-\mathbf{v}t,\mathbf{v})e^{-t/\tau} \tag{A.1}$$

with $f_0(\mathbf{r}-\mathbf{v}\tau s,\mathbf{v})$ given by the kinetic initial condition at $t = 0$. Solution to the boundary value problem ($t \gg \tau$) can be formally written as

$$f(\mathbf{r},\mathbf{v},t) = \int_0^{\infty} e^{-s(1+\tau v\nabla)} f^{eq}(\mathbf{r},\mathbf{v},t-\tau s)ds \tag{A.2}$$

after employing the shift operator $f(x + \Delta x) \equiv f(x)e^{\Delta x\nabla}$. Since boundary (surface) terms have been neglected, the solution in eqn (A.2) is only exact within the fluid bulk. It follows that hydrodynamic expressions derived from eqn (A.2) must be regarded as approximate within a thin layer adjacent to the wall; as a consequence, nontrivial boundary conditions (*e.g.*, effective slip) may be required in some flow regimes. A formal expression for the fluid velocity field can be obtained by taking the first velocity moment of $f(\mathbf{r},\mathbf{v},t)$:

$$\rho\mathbf{u}(\mathbf{r},t) = m\int \mathbf{v}d\mathbf{v}\int_0^{\infty} e^{-s(1+\tau v\nabla)} f^{eq}(\mathbf{r},\mathbf{v},t-\tau s)ds. \tag{A.3}$$

In the studied case of unidirectional shear flow ($\nabla \equiv \partial_y\mathbf{j}$) we have $\mathbf{u}(\mathbf{r},t) = u(y,t)\mathbf{i}$ and $\rho(\mathbf{r},t) = nm = \text{const}$; the equilibrium distribution then reads

$$f^{eq} = \frac{n}{(2\pi k_B\theta/m)^{3/2}}\exp\left(-\frac{m(v_x-u(y,t))^2}{2k_B\theta}\right)$$
$$\exp\left(-\frac{mv_y^2}{2k_B\theta}\right)\exp\left(-\frac{mv_z^2}{2k_B\theta}\right). \tag{A.4}$$

Use of eqn (A.4) in eqn (A.3) and evaluation of the Gaussian integrals lead to

$$u(y,t) = \int_0^{\infty} e^{-s} e^{\frac{s^2\tau^2\theta\nabla^2}{2}} u(y,t-\tau s)ds. \tag{A.5}$$

In order to construct a conservation equation for the fluid momentum we take partial time derivatives of eqn (A.5):

$$\frac{\partial u}{\partial t} = \tau\theta\int_0^{\infty} s e^{-s} e^{\frac{s^2\tau^2\theta\nabla^2}{2}} \nabla^2 u(y,t-\tau s)ds \tag{A.6}$$

$$\frac{\partial^2 u}{\partial t^2} = \theta\int_0^{\infty}\left[e^{-s}e^{\frac{s^2\tau^2\theta\nabla^2}{2}} + s\frac{\partial}{\partial s}\left(e^{-s}e^{\frac{s^2\tau^2\theta\nabla^2}{2}}\right)\right]\nabla^2 u(y,t-\tau s)ds. \tag{A.7}$$

We then combine eqn (A.6) and (A.7) and arrive at the following integro-differential equation:

$$\tau\frac{\partial^2 u}{\partial t^2} + \frac{\partial u}{\partial t} = \tau\theta\left(\nabla^2 u + \tau^2\theta\int_0^{\infty} s^2 e^{-s} e^{\frac{s^2\tau^2\theta\nabla^2}{2}} \nabla^4 u(y,t-\tau s)ds\right) \tag{A.8}$$

Provided that the BE-BGK equation is valid, the hydrodynamic relation in eqn (A.8) is formally applicable to arbitrary Knudsen or Weissenberg number regimes.

Asymptotic hydrodynamic approximations

Our goal here is to evaluate hydrodynamic approximations for the frequency limits $\omega\tau \to 0$ and $\omega\tau \to \infty$. We proceed by recasting eqn (A.8) as

$$\tau\frac{\partial^2 u}{\partial t^2} + \frac{\partial u}{\partial t} = \nu(1+\phi)\nabla^2 u \tag{A.9}$$

where $\nu = \tau\theta$ is the kinematic viscosity and

$$\phi = \tau^2\theta\int_0^{\infty} s^2 e^{-s\left(1+\tau\frac{\partial}{\partial t}\right)} e^{\frac{s^2\tau^2\theta\nabla^2}{2}} \nabla^2 ds. \tag{A.10}$$

For the case of unidirectional shear flow, we seek a single hydrodynamic mode

$$u(y,t) = u_0 e^{i\omega t} e^{-iky} \tag{A.11}$$

as the flow solution; ω and k are allowed to have both real and imaginary components. After defining $\mathrm{Kn} = \tau\sqrt{\theta}k \equiv \lambda k$, the dimensionless dispersion relation for eqn (A.9) becomes

$$(\omega\tau)^2 - i\omega\tau = \mathrm{Kn}^2(1+\phi) \tag{A.12a}$$

$$\phi = -\mathrm{Kn}^2 \int_0^\infty s^2 e^{-s(1+i\omega\tau)} e^{-\frac{s^2\mathrm{Kn}^2}{2}} ds. \tag{A.12b}$$

Note that the Knudsen number $\mathrm{Kn}(\tau\omega)$ is determined by the non-dimensional frequency, or Weissenberg number, $\mathrm{Wi} = \tau\omega$ according to a nontrivial dispersion relation. After expansion, the operator in eqn (A.12b) is $\phi = -\mathrm{Kn}^2 \int_0^\infty s^2 e^{-s(1+i\tau\omega)} \sum_{n=0}^\infty \frac{1}{n!}\left(-\frac{s^2\mathrm{Kn}^2}{2}\right)^n ds$. Using the identity $\int_0^\infty s^n e^{-As} ds \equiv \frac{n!}{A^{(n+1)}}$, we obtain

$$\begin{aligned}\phi &= \frac{1}{\mathrm{Kn}} \sum_{n=0}^\infty \frac{(-1)^{(n+1)}}{2^n} \frac{(2n+2)!}{n!} \left[\frac{\mathrm{Kn}}{(1+i\tau\omega)}\right]^{(2n+3)} \\ &= -\frac{2\mathrm{Kn}^2}{(1+i\tau\omega)^3} + \frac{12\mathrm{Kn}^4}{(1+i\tau\omega)^5} - \ldots \end{aligned} \tag{A.13}$$

the dispersion relation (A.11) can be then expressed as

$$(\omega\tau)^2 - i\omega\tau = \mathrm{Kn}^2 + \mathrm{O}\left(\frac{\mathrm{Kn}^4}{(1+i\omega\tau)^3}\right). \tag{A.14}$$

As expected, the Newtonian relation $-i\omega = \nu k^2$, with a kinematic viscosity $\nu = \tau\theta$, is recovered in the limit $\tau\omega \to 0$. In flow regimes where $\mathrm{Kn} < 1$ and $\tau\omega < 1$, the telegrapher's equation

$$\tau\frac{\partial^2 u}{\partial t^2} + \frac{\partial u}{\partial t} = \nu\nabla^2 u + \mathrm{O}(\mathrm{Kn}^4) \quad (\mathrm{Kn} \ll 1) \tag{A.15}$$

is obtained by neglecting contributions of order $\mathrm{O}(\mathrm{Kn}^4)$. In the case that $\mathrm{Kn} \gg 1$, we can estimate

$$\phi \sim -\mathrm{Kn}^2 \int_0^{1/\mathrm{Kn}} s^2 ds \sim -\frac{1}{\mathrm{Kn}} \tag{A.16}$$

and thus $(\omega\tau)^2 - i\omega\tau = \mathrm{Kn}^2 + \mathrm{O}(\mathrm{Kn})$. The hydrodynamic relation (A.15) becomes approximately valid in the high-frequency regime when $\omega\tau \gg \mathrm{Kn} \gg 1$;

$$\tau\frac{\partial^2 u}{\partial t^2} + \frac{\partial u}{\partial t} = \nu\nabla^2 u + \mathrm{O}(\mathrm{Kn}) \quad (\tau\omega \gg \mathrm{Kn} \gg 1).$$

Hence, we adopt the wave-diffusion eqn (A.17), known as the telegrapher's equation, as an approximate hydrodynamic relation in order to predict macroscopic features of the flow in both low- and high-frequency limits.

Acknowledgements

The authors acknowledge support from the U.S. National Science Foundation (NSF) through the Grants CBET-0755927, CMMI-0970071 (K.L.E., V.Y. and C.C.) and ECCS-0643178 (K.L.E.). S.R. was supported by CNST NIST.

References

1 K. L. Ekinci and M. L. Roukes, *Rev. Sci. Instrum.*, 2005, **76**, 061101.
2 H. G. Craighead, *Science*, 2000, **290**, 1532.
3 K. L. Ekinci, *Small*, 2005, **1**, 786–797.
4 P. Waggoner and H. Craighead, *Lab Chip*, 2007, **7**, 1238–1255.
5 N. V. Lavrik, M. J. Sepaniak and P. G. Datskos, *Rev. Sci. Instrum.*, 2004, **75**, 2229–2253.
6 K. L. Ekinci, X. M. H. Huang and M. L. Roukes, *Appl. Phys. Lett.*, 2004, **84**, 4469.
7 A. K. Naik, M. S. Hanay, W. K. Hiebert, X. L. Feng and M. L. Roukes, *Nat. Nanotechnol.*, 2009, **4**, 445–450.
8 Y. T. Yang, C. Callegari, X. L. Feng, K. L. Ekinci and M. L. Roukes, *Nano Lett.*, 2006, **6**, 583–586.
9 X. M. H. Huang, M. Manolidis, S. C. Jun and J. Hone, *Appl. Phys. Lett.*, 2005, **86**, 143104.
10 S. S. Verbridge, J. M. Parpia, R. B. Reichenbach, L. M. Bellan and H. G. Craighead, *J. Appl. Phys.*, 2006, **99**, 124304.
11 K. Jensen, K. Kim and A. Zettl, *Nat. Nanotechnol.*, 2008, **3**, 533–537.
12 A. N. Cleland and M. L. Roukes, *Nature*, 1998, **392**, 160–162.
13 D. Rugar, R. Budakian, H. J. Mamin and B. W. Chui, *Nature*, 2004, **430**, 329–332.
14 K. C. Schwab and M. L. Roukes, *Phys. Today*, 2005, **58**, 36–42.
15 M. D. LaHaye, O. Buu, B. Camarota and K. C. Schwab, *Science*, 2004, **304**, 74–77.
16 A. Schliesser, R. Riviere, G. Anetsberger, O. Arcizet and T. J. Kippenberg, *Nat. Phys.*, 2008, **4**, 415–419.
17 Y. T. Yang, K. L. Ekinci, X. M. H. Huang, L. M. Schiavone, M. L. Roukes, C. A. Zorman and M. Mehregany, *Appl. Phys. Lett.*, 2001, **78**, 162–164.
18 A. Husain, J. Hone, H. W. C. Postma, X. M. H. Huang, T. Drake, M. Barbic, A. Scherer and M. L. Roukes, *Appl. Phys. Lett.*, 2003, **83**, 1240–1242.
19 X. Feng, R. He, P. Yang and M. Roukes, *Nano Lett.*, 2007, **7**, 1953–1959.
20 T. R. Albrecht, P. Grutter, D. Horne and D. Rugar, *J. Appl. Phys.*, 1991, **69**, 668–673.
21 K. L. Ekinci, Y. T. Yang and M. L. Roukes, *J. Appl. Phys.*, 2004, **95**, 2682–2689.
22 A. Gupta, D. Akin and R. Bashir, *Appl. Phys. Lett.*, 2004, **84**, 1976–1978.
23 N. V. Lavrik and P. G. Datskos, *Appl. Phys. Lett.*, 2003, **82**, 2697–2699.
24 E. Forsen, G. Abadal, S. Ghatnekar-Nilsson, J. Teva, J. Verd, R. Sandberg, W. Svendsen, F. Perez-Murano, J. Esteve, E. Figueras, F. Campabadal, L. Montelius, N. Barniol and A. Boisen, *Appl. Phys. Lett.*, 2005, **87**, 043507.
25 P. Thiruvenkatanathan, J. Yan, J. Woodhouse, A. Aziz and A. A. Seshia, *Appl. Phys. Lett.*, 2010, **96**, 081913.
26 X. L. Feng, C. J. White, A. Hajimiri and M. L. Roukes, *Nat. Nanotechnol.*, 2008, **3**, 342–346.
27 A. Ayari, P. Vincent, S. Perisanu, M. Choueib, V. Gouttenoire, M. Bechelany, D. Cornu and S. T. Purcell, *Nano Lett.*, 2007, **7**, 2252–2257.
28 E. Buks and B. Yurke, *Phys. Rev. E: Stat., Nonlinear, Soft Matter Phys.*, 2006, **74**, 046619.
29 H. B. Peng, C. W. Chang, S. Aloni, T. D. Yuzvinsky and A. Zettl, *Phys. Rev. Lett.*, 2006, **97**, 087203.
30 X. M. H. Huang, C. A. Zorman, M. Mehregany and M. L. Roukes, *Nature*, 2003, **421**, 496.
31 A. N. Cleland and M. L. Roukes, *J. Appl. Phys.*, 2002, **92**, 2758–2769.
32 Q. P. Unterreithmeier, E. M. Weig and J. P. Kotthaus, *Nature*, 2009, **458**, 1001–1004.
33 M. Li, W. H. P. Pernice, C. Xiong, T. Baehr-Jones, M. Hochberg and H. X. Tang, *Nature*, 2008, **456**, 480–484.
34 H. P. Lang, M. K. Baller, R. Berger, C. Gerber, J. K. Gimzewski, F. M. Battiston, P. Fornaro, J. P. Ramseyer, E. Meyer and H. J. Güntherodt, *Anal. Chim. Acta*, 1999, **393**, 59–65.
35 M. K. Ghatkesar, E. Rakhmatullina, H.-P. Lang, C. Gerber, M. Hegner and T. Braun, *Sens. Actuators, B*, 2008, **135**, 133–138.
36 A. K. Gupta, P. R. Nair, D. Akin, M. R. Ladisch, S. Broyles, M. A. Alam and R. Bashir, *Proc. Natl. Acad. Sci. U. S. A.*, 2006, **103**, 13362–13367.
37 D. Lange, C. Hagleitner, A. Hierlemann, O. Brand and H. Baltes, *Anal. Chem.*, 2002, **74**, 3084–3095.
38 R. McKendry, J. Zhang, Y. Arntz, T. Strunz, M. Hegner, H. P. Lang, M. K. Baller, U. Certa, E. Meyer, H.-J. Güntherodt and C. Gerber, *Proc. Natl. Acad. Sci. U. S. A.*, 2002, **99**, 9783–9788.
39 P. S. Waggoner, M. Varshney and H. G. Craighead, *Lab Chip*, 2009, **9**, 3095–3099.

40 D. M. Karabacak, S. H. Brongersma and M. Crego-Calama, *Lab Chip*, 2010, **10**, 1976–1982.
41 D. M. Karabacak, V. Yakhot and K. L. Ekinci, *Phys. Rev. Lett.*, 2007, **98**, 254505.
42 K. L. Ekinci, D. M. Karabacak and V. Yakhot, *Phys. Rev. Lett.*, 2008, **101**, 264501.
43 V. Yakhot and C. Colosqui, *J. Fluid Mech.*, 2007, **586**, 249–258.
44 O. Svitelskiy, V. Sauer, N. Liu, K.-M. Cheng, E. Finley, M. R. Freeman and W. K. Hiebert, *Phys. Rev. Lett.*, 2009, **103**, 244501.
45 R. B. Bhiladvala and Z. J. Wang, *Phys. Rev. E: Stat., Nonlinear, Soft Matter Phys.*, 2004, **69**, 036307.
46 J. F. Vignola and J. A. Judge, *J. Appl. Phys.*, 2008, **104**, 124305.
47 D. Ramos, J. Mertens, M. Calleja and J. Tamayo, *Appl. Phys. Lett.*, 2008, **92**, 173108.
48 M. R. Paul and M. C. Cross, *Phys. Rev. Lett.*, 2004, **92**, 235501.
49 G. Karniadakis, A. Beskok, and N. Aluru, *Microflows and Nanoflows*, Springer, New York, 1st ed., 2005.
50 M. J. Martin and B. H. Houston, *Appl. Phys. Lett.*, 2007, **91**, 103116.
51 M. Gad-el-Hak, *J. Fluids Eng.*, 1995, **117**, 3–5.
52 L. D. Landau and E. M. Lifshitz, *Fluid Mechanics*, Butterworth-Heinemann, Oxford, 2nd ed., 1987.
53 G. K. Batchelor, *An Introduction to Fluid Dynamics*, Cambridge University Press, 2000.
54 E. O. Tuck, *J. Eng. Math.*, 1969, **3**, 29–44.
55 J. E. Sader, *J. Appl. Phys.*, 1998, **84**, 64–76.
56 L. D. Landau and E. M. Lifshitz, *Statistical physics. Pt.1, Pt.2*, Oxford: Pergamon Press, 1980.
57 C. Cercignani, *Mathematical methods in kinetic theory*, Plenum Press, 1990.
58 P. L. Bhatnagar, E. P. Gross and M. Krook, *Phys. Rev.*, 1954, **94**, 511–525.
59 S. Chen and G. D. Doolen, *Annu. Rev. Fluid Mech.*, 1998, **30**, 329–364.
60 H. Chen, S. Kandasamy, S. Orszag, R. Shock, S. Succi and V. Yakhot, *Science*, 2003, **301**, 633–636.
61 R. Benzi, S. Succi and M. Vergassola, *Phys. Rep.*, 1992, **222**, 145–197.
62 S. Chapman and T. G. Cowling, *The mathematical theory of non-uniform gases. an account of the kinetic theory of viscosity, thermal conduction and diffusion in gases*, 1970.
63 S. Chapman, *Proc. R. Soc. London, Ser. A*, 1916, **93**, 1–20.
64 H. Chen, S. Orszag, I. Staroselsky and S. Succi, *J. Fluid Mech.*, 2004, **519**, 301–314.
65 E. Lauga, M. Brenner, and H. Stone, Springer, New York, 2007; *chapter Microfluidics: The no-slip boundary condition*, pp. 1219–1240.
66 S. H. Kim, H. Pitsch and I. D. Boyd, *Phys. Rev. E: Stat., Nonlinear, Soft Matter Phys.*, 2008, **77**, 026704.
67 C. E. Colosqui, D. M. Karabacak, K. L. Ekinci and V. Yakhot, *J. Fluid Mech.*, 2010, **652**, 241–257.
68 J. H. Park, P. Bahukudumbi and A. Beskok, *Phys. Fluids*, 2004, **16**, 317–330.
69 P. Bahukudumbi and A. Beskok, *J. Micromech. Microeng.*, 2003, **13**, 873–884.
70 A. Cleland, *Foundations of Nanomechanics*, Springer, New York, 1st ed., 2003.
71 T. Kouh, D. Karabacak, D. H. Kim and K. L. Ekinci, *Appl. Phys. Lett.*, 2005, **86**, 13106.
72 A. Sampathkumar, T. W. Murray and K. L. Ekinci, *Appl. Phys. Lett.*, 2006, **88**, 223104.
73 I. Bargatin, E. B. Myers, J. Arlett, B. Gudlewski and M. L. Roukes, *Appl. Phys. Lett.*, 2005, **86**, 133109.
74 D. Karabacak, T. Kouh, C. C. Huang and K. L. Ekinci, *Appl. Phys. Lett.*, 2006, **88**, 193122.
75 I. D. Vlaminck, J. Roels, D. Taillaert, D. V. Thourhout, R. Baets, L. Lagae and G. Borghs, *Appl. Phys. Lett.*, 2007, **90**, 233116.
76 Q. P. Unterreithmeier, S. Manus and J. P. Kotthaus, *Appl. Phys. Lett.*, 2009, **94**, 263104.
77 N. Liu, F. Giesen, M. Belov, J. Losby, J. Moroz, A. E. Fraser, G. McKinnon, T. J. Clement, V. Sauer, W. K. Hiebert and M. R. Freeman, *Nat. Nanotechnol.*, 2008, **3**, 715–719.
78 R. Almog, S. Zaitsev, O. Shtempluck and E. Buks, *Phys. Rev. Lett.*, 2007, **98**, 078103.
79 W. J. Venstra and H. S. J. van der Zant, *Appl. Phys. Lett.*, 2008, **93**, 234106.
80 D. J. Evans and G. Morriss, *Statistical Mechanics of Nonequilibrium Liquids*, 2nd edition, Cambridge University Press, 2008.
81 A. Groisman and V. Steinberg, *Nature*, 2000, **405**, 53–55.
82 R. B. Bird, R. C. Armstrong, and O. Hassager, *Dynamics of Polymeric Liquids*, Vol. 1, Wiley, New York, 1977.
83 R. B. Bird, C. F. Curtis, R. C. Armstrong, and O. Hassager, *Dynamics of Polymeric Liquids Kinetic Theory*, Vol. 2, John Wiley, New York, 1987.
84 J. Magda and R. Larson, *J. Non-Newtonian Fluid Mech.*, 1988, **30**, 1–19.
85 M. Li, H. X. Tang and M. L. Roukes, *Nat. Nanotechnol.*, 2007, **2**, 114.
86 S. S. Verbridge, L. M. Bellan, J. M. Parpia and H. G. Craighead, *Nano Lett.*, 2006, **6**, 2109–2114.